lite-derived pigment concentrations has demonstrated that the algorithms used to relate the retrieved spectral radiances to phytoplankton pigment concentrations are accurate to within 30 to 40 percent [H. R. Gordon, D. K. Clark, J. W. Brown, O. B. Brown, R. H. Evans, *J. Mar. Res.* **40**, 2 (1982); R. C. Smith and K. S. Baker, *Mar. Biol.* **66**, 269 (1982); C. R. McClain *et al.*, *J. Geophys. Res.* **89**, 3705 (1984).

2. E. Firing, R. Lukas, J. Sadler, K. Wyrtki, *Science* **222**, 1121 (1983).
3. D. Halpern *et al.*, *ibid.* **221**, 1173 (1983).
4. The imagery presented in this report was processed on a satellite data- and image-processing system provided by R. Evans, O. Brown, J. Brown, and A. Lee of the University of Miami, Rosenstiel School of Marine and Atmospheric Sciences.
5. A series of 30 CZCS scenes of the eastern equatorial Pacific beginning in December 1978 and prior to the 1982–1983 El Niño have been examined in an effort to establish the scales of variability observed during normal years.
6. The western region is the area from 91°W to 92°50′W and from 2°S to 1°N; the eastern section is from 89°W to 91°W and from 2°S to 1°N.
7. A. Leetmaa *et al.*, *Trop. Ocean-Atmos. Newsl. No. 21* (1983), p. 11.
8. R. T. Barber and F. P. Chavez, *Science* **222**, 1203 (1983).
9. R. W. Owen, in *Analysis of Marine Ecosystems*, A. R. Longhurst, Ed. (Academic Press, New York, 1981), p. 197.
10. D. Limberger *et al.*, *Trop. Ocean-Atmos. Newsl. No. 21* (1983), p. 16.
11. T. Y. Canby, *Natl. Geogr.* **165**, 144 (1984).
12. A more detailed investigation of the relation between temporal and spatial variability of CZCS-derived phytoplankton distributions and the ecology of the Galápagos Islands is now under way.
13. Research support for G.F. was provided by NASA graduate researchers fellowship grant 33-015-802. We thank W. Hovis and L. Krone for their assistance in the analysis of the historical CZCS data; J. Sissala and P. Anderson for their help in scheduling the CZCS coverage during the 1982–1983 El Niño; R. Barber, J. Kogelschatz, and F. Chavez for their contributions; C. McClain for his support and encouragement; and all our colleagues who provided helpful comments and suggestions on early drafts. The moored measurements were obtained with support from the National Oceanic and Atmospheric Administration's Equatorial Pacific Ocean Climate Study program. Contribution No. 693 from the Pacific Marine Environmental Laboratory, National Oceanic and Atmospheric Administration. Contribution No. 400 from the Marine Sciences Research Center.

6 March 1984; accepted 9 May 1984

Densities of Liquid Silicates at High Pressures

Abstract. *Densities of molten silicates at high pressures (up to ~230 kilobars) have been measured for the first time with shock-wave techniques. For a model basaltic composition (36 mole percent anorthite and 64 mole percent diopside), a bulk modulus* K_s *of ~230 kilobars and a pressure derivative* (dK_s/dP) *of ~4 were derived. Some implications of these results are as follows: (i) basic to ultrabasic melts become denser than olivine- and pyroxene-rich host mantle at pressures of 60 to 100 kilobars; (ii) there is a maximum depth from which basaltic melt can rise within terrestrial planetary interiors; (iii) the slopes of silicate solidi* [(dT_m/dP), *where* T_m *is the temperature*] *may become less steep at high pressures; and (iv) enriched mantle reservoirs may have developed by downward segregation of melt early in Earth history.*

Knowledge of the properties of silicate liquids at high pressures and temperatures is fundamental to our understanding of the differentiation processes that occur within planetary interiors. Using the falling-sphere technique, Fujii and Kushiro determined the densities of a variety of silicate liquids at up to 20 kbar in a piston cylinder apparatus (*1*). Liquid silicate densities at high pressures have also been calculated by estimation of their elastic properties (*2, 3*). We report here the first shock-wave measurements of the densities of silicate liquids at high temperatures and pressures, extending by more than an order of magnitude (to 235 kbar) the maximum pressure at which the densities have been determined. Our motivations for this work included the following:

1) The rates of melt migration and segregation within partially molten source regions in planetary interiors depend on the difference in density between the melt and the coexisting solids. In addition, the sign of the density contrast between the melt and the coexisting residual crystals determines whether melt will migrate upward or downward (*2*). Magma may move from its source by percolation, in cracks, or as diapirs. In each of these cases, the density contrast between melt and solid enters into the velocity with which the magma moves and thus places important constraints on the thermal and chemical evolution of rising (or sinking) magmas.

2) The slope of the solidus, (dT_m/dP), where T_m is temperature and P is pressure, depends upon ΔV_r (the volume change of the reaction defining the solidus). Thus the pressure dependence of the density contrast between coexisting phases along the solidus is an important factor in the variation of the position of the solidus with pressure and consequently in the melting behavior of planetary mantles.

3) The structures of silicate melts at high pressures and temperatures have been predicted by molecular dynamics simulations. These simulations also model the density and transport properties of silicate melts (*4*). Density measurements at high pressures can be compared with those derived from the simulations to place constraints on the interatomic potentials that are critical to the calculations and hence to refine calculated structural models and transport properties.

The composition that we used for our initial experiments is the 1-atm eutectic composition in the system anorthite-diopside ($An_{0.36}$ $Di_{0.64}$, where the subscripts represent mole fractions). This composition is used as an analog for natural basalt and differs from it mainly in the absence of iron and alkalis. Ultrasonic measurements (*5*) at 1 atm and 1400°C yield a bulk modulus of ~230 kbar for this composition.

The pressure and density (ρ) of a material in shock-wave experiments are determined from the Rankine-Hugoniot equations (*6*). The shock wave is generated in the molten sample encapsulated in molybdenum by impact of a metal flyer plate that has been accelerated to high velocity (1 to 2.5 km/sec) in a 40-mm propellant gun (*7*). A schematic representation of the experimental target, just prior to projectile impact, is shown in Fig. 1 (*8, 9*). During these experiments, the quantities measured are shock velocity (U) and particle velocity (u). One can calculate the 1-atm density (ρ_0) by using partial molar volumes reported by Nelson and Carmichael (*10*). The particle velocity is determined by measurement of projectile velocity and subsequent impedance match with the sample (*9*). One obtains the shock velocity by measuring the time difference between the entrance and exit of the shock front through the sample (*11, 12*).

The results are shown in Table 1 and Fig. 2. The U-u data can be fit by a straight line given by

$$U = (2.94 \pm 0.05 \text{ km/sec}) + (1.29 \pm 0.06)u$$

This experimental fit to the Hugoniot is shown in the inset of Fig. 2. From the analysis developed by Ruoff (*13*), we calculate an isentropic, 1-atm bulk modulus, $K_S^0 = \rho(\partial P/\partial \rho)_S = 226 \pm 8$ kbar, and a pressure derivative, $K_S' = dK_S/dP = 4.15 \pm 0.24$. The value of K_S^0 is in good agreement with the value calculated from the measured ultrasonic velocity (212 to 243 kbar) (*5, 14*). For typical mantle minerals K_S^0 is ~1.2 to 2.1 mbar and K_S' ~4 to 7 (*15*).

With increasing P, crystalline silicates undergo phase changes leading to abrupt increases in ρ as the structure transforms to the closer packing stable at elevated P. Waff (*16*) suggested that similar abrupt increases in ρ would occur in silicate liquids as coordination changes such as ${}^{IV}Al^{3+} \rightarrow {}^{VI}Al^{3+}$ and ${}^{IV}Si^{4+} \rightarrow {}^{VI}Si^{4+}$ occurred. However, silicate liquids could achieve substantial compac-

Table 1. Molten $An_{0.36}Di_{0.64}$ Hugoniot data (T_0 = 1400°C, ρ_0 = 2.615 g/cm^3).

Shot No.	Flyer plate material	Measured		Calculated		
		Impact velocity (km/sec)	Shock velocity (km/sec)	Particle velocity (km/sec)	Hugoniot pressure (kbar)	Hugoniot density (g/cm^3)
592	Al	1.05 ± 0.02	3.59 ± 0.04	0.44 ± 0.01	41.0 ± 0.9	2.978 ± 0.026
593	Al	1.50 ± 0.03	3.65 ± 0.04	0.65 ± 0.02	65.0 ± 1.4	3.176 ± 0.030
605	Al	2.00 ± 0.04	4.06 ± 0.10	0.88 ± 0.02	93.0 ± 2.9	3.33 ± 0.04
607	W	1.80 ± 0.03	5.20 ± 0.05	1.73 ± 0.03	235.4 ± 5.0	3.92 ± 0.05

tion by a continual distortion of the tetrahedral network or by gradual coordination changes rather than by the abrupt coordination changes characteristic of solids. Raman spectroscopy carried out on glasses quenched from jadeite melts at *P* up to 40 kbar does indeed suggest that the Al(Si)–O–Al(Si) bond angles in the tetrahedral network decrease continuously and that at this *P* aluminum and silicon are still essentially entirely in tetrahedral coordination (*17*). Recent nuclear magnetic resonance results from albite glasses quenched from melts at high pressures suggest that, when Al^{3+} enters sixfold coordination in melts, it does so over a wide *P* range (*18*). Molecular dynamics simulations have also suggested that structural changes in melts, and especially silicon and aluminum coordination numbers, change gradually and continuously as pressure increases to several hundred kilobars (*4*) rather than abruptly over narrow *P* intervals (*19*). Our results are consistent with gradual and continuous structural changes, since the data can be fit by a single compression curve (a straight line in *U*-*u* space). In addition, the unexpectedly low value of K_s' (*2, 3*) can be rationalized on the basis of continuous structural changes taking place in the melt with increasing *P*.

These results have some far-reaching implications for differentiation within terrestrial planetary interiors by igneous processes.

1) Using the values of K_s and K_s' derived from our experiments (*20*), we predict that the density of volatile-poor, basic to ultrabasic melts of the mantle would overtake the bulk density of the

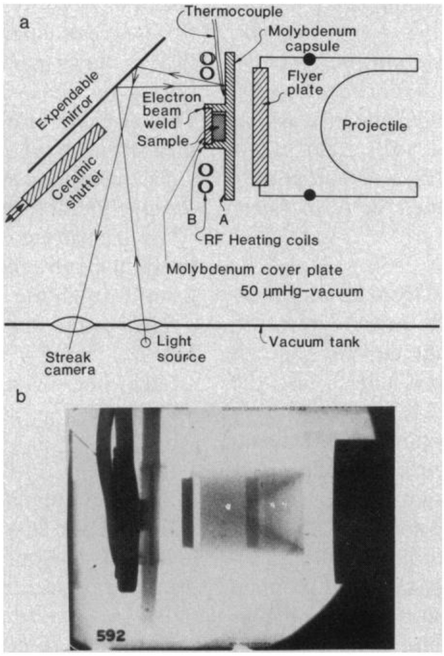

Fig. 1 (left). (a) Shock experiment for molten silicate target. The silicate sample is encapsulated between a molybdenum driver plate and a molybdenum cover plate. The metal capsule is heated by induction (*8*) and acts as a furnace. Measurement of the projectile velocity via double-flash (30 nsec) x-ray shadowgraph (12 to 30 µsec apart) allows determination of the particle velocity by impedance match with the molybdenum driver plate (*9*). The temperature of the molten sample, monitored by a platinum-rhodium thermocouple, determines the initial density (*10*). One determines the shock velocity by measuring the time difference between the shock arrival at planes A and B (*11*). Shock propagation time through the molybdenum cover plate must be subtracted from sample plus cover plate, introducing an error of 0.3 percent in the measured shock velocity. A ceramic shutter covers the expendable mirror until ~1 second before the shot is fired (*12*). (b) Double x-ray shadowgraph of the projectile during its flight toward the target.

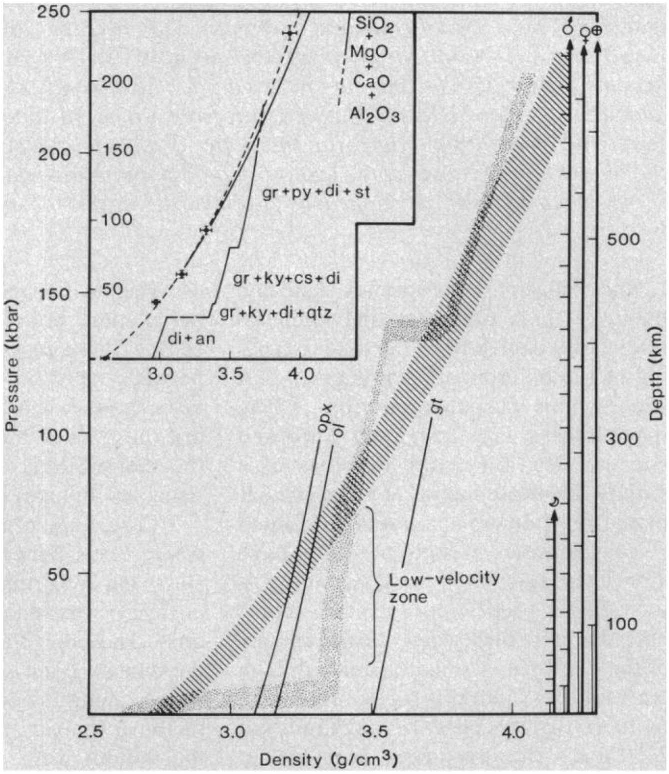

Fig. 2 (right). Density of basic silicate melt compared with that of Earth's mantle and likely liquidus minerals olivine (ol), orthopyroxene (opx), and garnet (gt). The hachured band represents the range of melt densities expected in the compression of basaltic compositions from an average mid-ocean ridge basalt (ρ_0 = 2.7 g/cm^3) to komatiite (ρ_0 = 2.8 g/cm^3) (*21, 22*) based on the values of K_s and K_s' derived from our work. Adiabatic compression curves are shown for three possible liquidus minerals (*23*). The stippled band represents the range of density-depth relations in Earth derived from two recent seismological whole-Earth models (PEM and PREM) and a density model based on free oscillation data (*24*). Depth scales are shown at the right for the major terrestrial planets and Earth's moon (*25*); the tick marks on each scale are at 100-km intervals. The inset shows dynamic compression data for $An_{0.36}Di_{0.64}$ at an initial temperature of 1400°C (ρ_0 = 2.615 ± 0.025). The dashed line passing through the data points is a Hugoniot fit to the experimental points. The solid line adjacent to the Hugoniot is calculated from the Birch-Murnaghan equation with K_S^0 = 226 kbar and K_s' = 4.15. This curve deviates from the Hugoniot only above ~100 kbar where shock heating becomes important. Adiabatic compression curves of the expected solid of this bulk composition are also shown for an initial temperature of 1400°C. Above 80 kbar the phase assemblage is uncertain but is probably well approximated by the lefthand curve to ~150 kbar. The rightmost curve is a maximum possible density estimate based on an assemblage of high-pressure-phase mixed oxides. Abbreviations: an, anorthite; di, diopside; qtz, quartz; cs, coesite; ky, kyanite; gr, grossular; py, pyrope; st, stishovite; ☽, moon; ⊕, Earth; ♂, Mars; and ♀, Venus.

residual solid at moderate P, 60 to 100 kbar. Basaltic liquid compression curves fall within the hachured band in Fig. 2. The range of 1-atm ρ values corresponds to that expected for picritic mid-ocean ridge basalt (2.7 g/cm^3) to komatiite (2.8 g/cm^3) at their liquidi (*21–23*). The liquids become denser than magnesian olivine and orthopyroxene, which are probable residual phases, at P from 40 to 70 kbar. Furthermore, the liquids become denser than the bulk mantle [derived from whole Earth seismological models (*24, 25*)] between 60 and 100 kbar. We propose that the lack of density contrast between melt and coexisting solid over this P range could lead to stabilization of partially molten zones in the region of the low-velocity zone of the present Earth (*2*).

2) There is a maximum depth from which volatile-poor basaltic magma produced by partial melting of ultrabasic mantle material can be derived; the estimate of this depth is based on the requirement of a positive density contrast to drive upward melt migration (*2*). For Earth and Venus, assuming an average 1-atm basaltic magma density of 2.75 g/cm^3 derived from a mantle where Mg/(Fe + Mg) $\sim$ 0.9 (*26*), this depth is about 300 km. For Mars, a much smaller planet, which may have a more iron-rich mantle [Mg/(Fe + Mg) $\sim$ 0.7 to 0.8], this depth would be much greater, about 1000 km (*27*). Internal pressures within the moon are not expected to be high enough to lead to a density crossover for a primitive basaltic composition (*28*).

3) A decrease in the density contrast between liquid and coexisting solids is expected to lead to a decrease in the slope of the solidus (dT_m/dP), which, in the absence of excess volatiles, is positive for all likely mantle rocks at low P. For congruent melting of a single mineral, the slope of the solidus flattens with increasing P as $\Delta V_r \rightarrow 0$. For incongruent melting, melting involving solid solutions, or melting of a polymineralic assemblage, however, dT_m/dP may be positive even though the melt is denser than some or all of the residual solid phases. Thus, care must be taken in using our results to infer the slope of a peridotite solidus at high P, since a very dense phase, garnet, is an important participant in likely melting reactions and since the liquid compositions at peridotite solidus are not well known at high P. If the slopes of the source rock and basalt solidi remain positive and are greater than the prevailing geothermal gradient, any dense melt percolating downward will begin to crystallize and presumably may not move very far. However, if the slopes of the solidi do become flat or negative, there could be an increase in the amount of melt with increasing depth, both from concentration of downward-percolating liquids and from the decrease in solidus temperatures.

Our analysis implies that the slopes of the solidi of congruently melting silicates with octahedral Si^{4+} (for example, $MgSiO_3$ perovskite) at high pressures are less than those of silicates found in the shallow mantle [dT_m/dP for enstatite at 1 atm is 13°C per kilobar (*29*)] and that their solidi may indeed become less steep. Recent shock temperature measurements confirm this; for stishovite at 700 kbar and 4200°C, dT_m/dP was inferred to be 1.1° ± 0.5 per kilobar (*30*). Extrapolating our results, we calculate that the density of liquid $MgSiO_3$ at 3000°C would increase from 2.31 g/cm^3 at 1 atm to 4.08 g/cm^3 at 400 kbar (*31*). At 400 kbar, $MgSiO_3$ perovskite would have a ρ of 4.63 g/cm^3 at room temperature and 4.10 g/cm^3 at 3000°C (*32*). If we assume congruent melting and an entropy of melting of $\sim R$ (8.3 joule/mole atom K) (*33*), $dT_m/dP = 0.1$°C per kilobar. With the melting-point estimate of Ohtani (*34*) for $MgSiO_3$ perovskite of 2900°C at 230 kbar, we can estimate the melting point at 400 kbar to be $\sim$3500°C. Despite the substantial extrapolations required for this calculation, we suggest that there may be a maximum in the solidus of perovskite in the vicinity of 400 kbar and that, at the very least, the slope of the solidus will be very small. This further implies that the temperature of the lower mantle is constrained to be $<$3500°C in the absence of partial melt.

4) That a silicate liquid may become more dense than its surroundings at high P allows not only for the possibility of retaining magma within planetary interiors but also for concentrating it at depth by downward segregation. Some implications of a laterally extensive, dense, magnesian melt layer for the genesis of komatiites were recently discussed by Nisbet and Walker (*22*). Stolper and his co-workers (*2*) and Ohtani (*34*) also discussed possible implications of dense melts at depth for komatiite genesis. During early Earth history when the heat production from radioactive decay was presumably higher than today (*35*), it is likely that there was a higher degree of partial melting globally and that it extended to greater depths than in the present Earth. Because the likely dominant residual minerals, olivine and orthopyroxene, would be expected to float in basic melts at pressures greater than $\sim$40 to 70 kbar, stable chemical stratification could occur. If basic to ultrabasic melts could flow downward in this way, such a process could lead to the development of a residual layer rich in olivine and orthopyroxene ("peridotitic" layer) underlain by a deep layer rich in clinopyroxene and garnet ("eclogitic" layer) in the upper mantle. Recent fits of elastic models to seismic velocity models lend credence to the idea of a stratified upper mantle having a lower proportion of olivine below $\sim$220 km than was previously thought (*36*). The development of such a zone by downward melt migration could have important consequences for the thermal evolution of the early Earth. It would limit the transport of heat toward the surface by magmatic activity, would interfere with convection patterns that might otherwise develop, and would allow the segregation of heat-producing incompatible elements (for example, potassium, uranium, and thorium) into a deep layer.

SALLY M. RIGDEN
THOMAS J. AHRENS
EDWARD M. STOLPER
*Division of Geological and
Planetary Sciences, California Institute
of Technology, Pasadena 91125*

References and Notes

1. T. Fujii and I. Kushiro, *Carnegie Inst. Washington Yearb.* **76**, 419 (1977).
2. E. Stolper, D. Walker, B. H. Hager, J. F. Hays, *J. Geophys. Res.* **86**, 6261 (1981); D. Walker, E. Stolper, J. F. Hays, *ibid.* **83**, 6005 (1978).
3. E. Ohtani, *Earth Planet. Sci. Lett.* **67**, 261 (1984); C. T. Herzberg, *ibid.*, p. 249.
4. L. V. Woodcock, C. A. Angell, P. A. Cheeseman, *J. Chem. Phys.* **65**, 1565 (1976); C. A. Angell, P. A. Cheeseman, S. Tamaddon, *Science* **218**, 885 (1982); Y. Matsui and K. Kawamura, *Nature (London)* **285**, 648 (1980); ______, Y. Syono, in *High Pressure Research in Geophysics*, S. Akimoto and M. H. Manghnani, Eds. (Center for Academic Publications, Tokyo, 1982), pp. 511–524.
5. M. L. Rivers and I. S. E. Carmichael, *Eos* **62**, 1065 (1981); *ibid.* **63**, 1136 (1982).
6. G. E. Duvall and G. R. Fowles, in *High Pressure Physics and Chemistry*, R. S. Bradley, Ed. (Academic Press, New York, 1963), vol. 2, pp. 209–291.
7. T. J. Ahrens, J. H. Lower, P. L. Lagus, *J. Geophys. Res.* **76**, 518 (1971).
8. The sample is hung and aligned in the impact tank and heated under vacuum to the requisite temperature with a water-cooled copper induction coil powered by a 10-kW Lepel high-frequency induction heating generator.
9. The impedance match method relies on continuity of stress and particle velocity at the flyer-driver and driver-sample interfaces [(*6*); R. G. McQueen, S. P. Marsh, J. W. Taylor, J. N. Fritz, W. J. Carter, in *High Pressure Impact Phenomena*, R. Kinslow, Ed. (Academic Press, New York, 1970), pp. 293–417].
10. S. A. Nelson and I. S. E. Carmichael, *Contrib. Mineral. Petrol.* **71**, 117 (1979).
11. One can determine the transit time by observing the polished rear surfaces of the molybdenum capsule on a continuously writing Beckman-Whitely streak camera (model 339). Because the molybdenum is polycrystalline, the reflection of a shock wave at the free surface results in a reorientation of the crystallites and a change in reflectivity. Illumination is accomplished by a 5-kV, 100-μsec xenon flash lamp synchronized with impact. The firing sequence is arranged so that the camera shutter opens $\sim$50 msec prior to impact to prevent fogging of the film by self-illumination of the hot target.
12. Retraction of the ceramic shutter is activated by a double-acting Bimba model SSRD-173-DNR-B

air cylinder under a pressure of ~1.5 bar controlled by air lines external to the impact chamber.

13. A. L. Ruoff, *J. Appl. Phys.* **38**, 4976 (1967).
14. Relaxation times in liquids are strongly dependent on the liquid viscosity. For an alkali olivine basalt at 1300°C and 1 atm, relaxation times are inferred to be <2 nsec [C. S. Rai, M. H. Manghnani, K. W. Katahara, *Geophys. Res. Lett.* **8**, 1215 (1981)] and viscosity η is inferred to be ~55 poises (calculated from the data of Y. Bottinga and D. F. Weill [*Am. J. Sci.* **272**, 438 (1972)]. At 1400°C, $\eta \sim 35$ poise for $An_{0.36}Di_{0.64}$. If the relaxation time is <2 nsec, the ultrasonically measured 1-atm bulk modulus should represent the relaxed value. Good agreement with the shock bulk modulus suggests that we also measure the relaxed value in our experiment.
15. R. Jeanloz and A. B. Thompson, *Rev. Geophys. Space Phys.* **21**, 51 (1983).
16. H. S. Waff, *Geophys. Res. Lett.* **2**, 193 (1975).
17. S. K. Sharma, D. Virgo, B. Mysen, *Am. Mineral.* **64**, 779 (1979).
18. E. Ohtani, F. Taulelle, C. A. Angell, in preparation.
19. A. Boettcher, Q. Guo, S. Bohlen, B. Hanson, *Geology* **12**, 202 (1984).
20. The application of our results to complex, natural liquid compositions is, we believe, justified in view of the weak dependence of elastic properties of silicate melts on bulk composition observed in ultrasonic experiments (*2*, *5*).
21. E. Stolper, *Contrib. Mineral. Petrol.* **74**, 13 (1980).
22. E. G. Nisbet and D. Walker, *Earth Planet. Sci. Lett.* **60**, 105 (1982).
23. The Birch-Murnaghan adiabats shown are for magnesian olivine (90 mole percent forsterite), orthopyroxene (90 mole percent enstatite), and mantle garnet [ρ from F. R. Boyd and R. H. McCallister, *Geophys. Res. Lett.* **3**, 509 (1976)] at an initial temperature of 1400°C. Elastic properties, ρ and thermal expansivity for olivine and orthopyroxene are from Jeanloz and Thompson (*15*); for garnet, the data of N. Soga [*J. Geophys. Res.* **72**, 4227 (1967)] and B. J. Skinner [*Geol. Soc. Am. Mem.* **97**, 75 (1966)] were used.
24. PREM (Preliminary Reference Earth Model): A. M. Dziewonski and D. L. Anderson, *Phys. Earth Planet. Inter.* **25**, 297 (1981). PEM (Parameterized Earth Models): A. M. Dziewonski, A. L. Hales, E. R. Lapwood, *ibid.* **10**, 12 (1973). Density model from free oscillations: T. H. Jordan and D. L. Anderson, *Geophys. J. R. Astron. Soc.* **36**, 411 (1975).
25. Z. N. Zharkov and V. P. Trubitsyn, in *Physics of Planetary Interiors*, W. B. Hubbard, Ed. (Pachart, Tucson, 1978), vol. 6, pp. 335 and 338.
26. Typical estimates of Mg/(Mg + Fe) (molar) for Earth are 0.9 [for example, Basaltic Volcanism Study Project, *Basaltic Volcanism on the Terrestrial Planets* (Pergamon, New York, 1981)]. Recent chemical analyses made by Venera 13 and Venera 14 suggest strong similarities between Venusian and terrestrial surface rocks [V. L. Barsukov *et al.*, *Geochem. Int.* **19** (No. 4), 1 (1982)] and lead us to use a similar internal composition for Venus.
27. Estimates of Mg/(Mg + Fe) (molar) in Mars and the composition of model Mars magma were taken from T. R. McGetchin and J. R. Smyth [*Icarus* **34**, 512 (1978)]. The initial ρ of model Mars basalt is slightly higher (~2.77 g/cm^3) than primitive terrestrial basalt because of higher iron content. However, mantle ρ is inferred to be on the order of 0.2 g/cm^3 higher on Mars up to a pressure of ~125 kbar because of the mantle's higher iron content [see the Basaltic Volcanism Study Project (*26*)]. Thus the pressure at which $\Delta\rho \rightarrow 0$ for Mars would be expected to be higher than on Earth or Venus.
28. The composition of a primitive lunar magma, a supposed parent to the lunar crust, was taken from A. E. Ringwood, *Origin of the Earth and Moon* (Springer, New York, 1979). An inferred lunar density-depth profile is given in the Basaltic Volcanism Study Project (*26*).
29. F. R. Boyd, J. L. England, B. T. C. Davis, *J. Geophys. Res.* **69**, 2101 (1964).
30. G. A. Lyzenga *et al.*, *ibid.* **88**, 2431 (1983).
31. The 1-atm ρ of $MgSiO_3$ liquid is calculated by extrapolation of ρ measurements of J. W. Tomlinson, M. S. R. Haynes, and J. O'M Bockris [*Trans. Faraday Soc.* **54**, 1822 (1958)].
32. For $MgSiO_3$ perovskite $K_s^0 = 2620$ kbar and $K_s' = 4$ (*15*). A third-order Birch-Murnaghan equation of state was used in calculating high-pressure ρ values and a thermal expansion, $\alpha = (0.2367 \times 10^{-4}) + (0.5298 \times 10^{-8}\ T) - 0.5702\ T^{-2}\ K^{-1}$ [H. Watanabe, in *High Pressure Research in Geophysics*, S. Akimoto and M. H. Manghnani, Eds. (Center for Academic Publications, Tokyo, 1982), p. 450], was assumed.
33. S. M. Stishov, *Sov. Phys. Usp.* **17**, 625 (1975).
34. E. Ohtani, *Phys. Earth Planet. Inter.* **33**, 12 (1983).
35. N. H. Sleep, *J. Geol.* **87**, 671 (1979).
36. J. D. Bass and D. L. Anderson, *Geophys. Res. Lett.* **11**, 229 (1984); H. Sawamoto, D. J. Weidner, S. Sasaki, M. Kumazawa, *Science* **224**, 749 (1984).
37. We are grateful to L. T. Silver for use of the Lepel radio-frequency generator and for his continued interest. We have benefitted from discussions with and comments from D. L. Anderson, J. D. Bass, A. Boettcher, I. S. E. Carmichael, H. Eissler, R. Hill, M. H. Manghnani, S. A. Morse, O. Navon, R. O'Connell, E. Ohtani, F. Richter, M. L. Rivers, D. R. Scott, D. J. Stevenson, and D. Walker. Supported by NSF grant EAR80-18819. Contribution No. 4112, Division of Geological and Planetary Sciences, California Institute of Technology.

11 June 1984; accepted 10 July 1984

The Oceanic Carbonate System: A Reassessment of Biogenic Controls

Abstract. *Fluxes of biogenic carbonates moving out of the euphotic zone and into deeper undersaturated waters of the North Pacific were estimated with free-drifting sediment traps. Short-duration (1 to 1.5 day) sampling between 100 and 2200 meters points to a major involvement in the oceanic carbonate system by a class of organisms which had been relegated to a secondary role—aragonitic pteropods. Pteropod fluxes through the base of the euphotic zone are almost large enough to balance the alkalinity budget for the Pacific Ocean. Dissolution experiments with freshly collected materials shed considerable light on a mystery surrounding these labile organisms: although plankton collections from net tows almost always contain large numbers of pteropods, these organisms are never a major component of biogenic materials in long-duration sediment trap collections. Their low abundance in long-duration collections results from dissolution subsequent to collection. Short-duration sampling showed significant increases in the ratio of calcitic foraminifera to aragonitic pteropods in undersaturated waters, indicating the more stable mineralogic form, calcite, was preserved relative to aragonite. Approximately 90 percent of the aragonite flux is remineralized in the upper 2.2 kilometers of the water column.*

The oceans constitute a substantial reservoir for anthropogenic CO_2 (*1*). The behavior of this reservoir, including its internal physical and chemical processes, is expected to significantly influence the rate of atmospheric CO_2 buildup and thereby the earth's future climate (*2*, *3*). In light of this expectation, the marine CO_2 system has been extensively investigated. Field and laboratory investigations (*4–7*) have provided a detailed picture of the oceanic distributions of total CO_2, dissolved carbonate ions, and the saturation state of particulate carbonates. Nevertheless, important facets of the marine CO_2 system remain poorly understood. Little is known about the rate of removal of CO_2 from the surface ocean via biogenic particulate carbonates and about the delivery rates of these materials to the undersaturated deep ocean.

For the Pacific Ocean, which constitutes approximately one-third of the earth's total area, there is an extreme paucity of carbonate flux data. Published data include information obtained at a single station in the central Pacific (*8*, *9*), and at another station in the western North Pacific (*10*). With an unusually shallow carbonate saturation horizon (*11*) and an alkalinity anomaly in intermediate and deep water attributable to the dissolution of biogenic carbonates (*12*), particulate carbonates take on special importance in the Pacific Ocean.

The feature that makes carbonate fluxes in the Pacific of special interest also complicates the interpretation of flux measurements. Dissolution of sedimenting aragonite particulates in the water column begins at relatively shallow depths (*11*) and generally proceeds rapidly below 100 m (*13*). As a consequence, long-duration sediment-trap deployments can seriously underestimate the mass fluxes of labile carbonates. In order to minimize this problem, our free-drifting sediment traps were deployed for less than 40 hours. This sampling period, quite brief compared to the deployment times in earlier investigations (*8–10*), permitted the deployment of numerous sediment traps along an extensive section of the western Pacific (Fig. 1).

The vertical fluxes of particulate matter were estimated with free-drifting sediment traps (cross sectional area, 0.66 m^2) patterned after the cone design of Soutar *et al.* (*14*). In our system, trapped materials are concentrated in a Teflon receptacle (2.5 cm in diameter) at the bottom of the trap's cone (*15*). Prior to retrieval, the Teflon cup and its contents were isolated from further inputs by a double-ball valve seal activated by an electronic release.

The total particle flux was determined